Supporting information for

Thermal runaway-free Ah-level Na-ion battery

Jiao Zhang[1], Lin Zhou[1], Haibo Wang[1,2], Suting Weng[1], Shuai Han[1], Yang Yang[1,2], Yuan Liu[1,2], Zhao Chen[1,2], Xubin Wang[1,2], Feixiang Ding[1,4], Fei Xie*[1], Huican Mao*[6], Xuefeng Wang[1], Yaxiang Lu*[1,4], Liquan Chen[1], Yong-Sheng Hu*[1,2,3,4,5]

[1]Key Laboratory for Renewable Energy, Beijing Key Laboratory for New Energy Materials and Devices, Beijing National Laboratory for Condensed Matter Physics, Institute of Physics, Chinese Academy of Sciences, Beijing 100190, China

[2]College of Materials Science and Optoelectronic Technology, University of Chinese Academy of Sciences, Beijing 100049, China

[3]HiNa Battery Technology Co., Ltd., Beijing, China.

[4]Huairou Division, Institute of Physics, Chinese Academy of Sciences, Beijing 101400, China

[5]Yangtze River Delta Physics Research Center Co. Ltd, Liyang 213300, China

[6]Department of Materials Science and Key Laboratory of Automobile Materials, MOE, Jilin University, Changchun 130012, China

Methods

Materials preparation

The layered cathode and carbon anode materials are from HiNa Battery Technology Co., Ltd.. Composition of the cathode (total mass loading on a single side of electrode: ~16 mg cm^{-2}) slurry was 92 wt%. active materials, 4 wt% conductive carbon and 4 wt% binder. The mass loading of only active cathode materials is ~14.7 mg cm^{-2}. The electrode slurries were casted on Al foil followed by a drying process under vacuum. Composition of the anode (total mass loading on a single side of electrode: ~7.0 mg cm^{-2}) slurry was 92 wt%. active materials, 4 wt% conductive carbon and 4 wt% binder. The mass loading of only active cathode materials is ~6.44 mg cm^{-2}. Analytical grade solvents were purchased from Shanshan Technology (purity, >99.95%). Sodium salts were purchased from Rolechem (purity, >99.95%). All chemical reagents are used directly without any further purification. The electrolytes were prepared using the stoichiometric ratio of solvent and metal salt in the glovebox, where the moisture and oxygen contents are controlled less than 0.5 ppm.

Electrochemical measurements

All coin cells were assembled in the Ar-filled glovebox using the CR-2032 type coin cell. The amount of electrolyte used for a coin cell is 50 μl. Glass fibre (Whatman GF/A) plus Celgard membrane was utilized as the separator. The 26700-type cylindrical cells and 18650-type cylindrical cells were assembled in a dry room with -50ºC dew point. The charge and discharge tests of full cells were performed on the Land battery test systems (CT3001A or CT2001A) or Neware battery test system (CT-4008). LSV measurements were obtained on a CHI 600E electrochemical workstation (0.1 mV s^{-1}). LSV measurements were obtained from the Na||stainless steel cells using different electrolytes at a scan rate of 0.1 mV s^{-1} from the -0.1V to 5.2V.

Characterizations

All MS data were acquired on an LTQ Orbitrap XL hybrid mass spectrometer

(Thermo Fisher Scientific, San Jose, CA, USA). A DC bias of 2000 V was applied at the nozzle to generate an electrospray jet. The Orbitrap ion transfer capillary was held at 275℃, and the capillary and tube lens voltages were set at 0 V to avoid unnecessary in-source fragmentation. The resolution was set to 60,000 for all analyses. All data were analyzed using the Qual Browser feature of the XcaliburTM program (version 4.1, Thermo Fisher Scientific, San Jose, CA). The morphologies of the samples were investigated by TEM (FEI Tecnai G2 F20). Cryo-TEM characterizations were carried out using a JEOL JEM-F200 microscope with a cryo transfer holder (Fischione, model 2550) under cryogenic temperatures (100 K) at 200 kV. The electronic conductivity values were obtained from a four-point-probe conductivity metre (MCP-PD51). The surface chemical state was determined by XPS using a PHI 5000 VersaProbe III instrument (Scanning ESCA Microprobe) with Al Kα X-ray source, 15 kV X-ray beam (analysis area: 200 μm × 200 μm) and Ar^+ rate: 3.9 nm min^{-1} for SiO_2 etching (sputtering). All spectra were calibrated with the C1s photoemission peak at 284.8 eV to correct for the charging effect. FTIR was performed by a Bruker VERTEX 80 V spectrophotometer in attenuated total reflection mode (not transmission mode) in a glove box. TOF-SIMS analysis was conducted with a PHI nanoTOF II spectrometer with a 30 keV Bi_1^+ acquisition ion beam and a 1 kV Cs^+ sputtering ion beam for electrodes, respectively. During depth profiling, the typical acquisition area was 200 μm × 200 μm and centred within the Ar^+ 500 μm × 500 μm sputtered area. The DSC tests were conducted on a differential scanning calorimeter (Mettler-Toledo, DSC1) in Ar atmosphere at a scanning rate of 5 ℃ min^{-1} from 30 ℃ to 400 ℃. Nail penetration tests: a nail with a diameter of 3 mm was punctured through the battery. The ARC tests were carried out using a commercial ARC system (THT EV+, Thermal Hazard Technology, U.K.) with a detection sensitivity of 0.01 ℃ min^{-1}. For the HWS (Heat-Wait-Search) stage, the temperature is increased by 5 ℃ increments. At each increment, the temperature is held constant for 30 minutes. The process continues until the highest temperature of 300 ℃ is reached. The thermal abuse test was conducted in a heated explosion-proof chamber. The chamber was heated from room temperature to 130 ℃ at a rate of

5 ℃/min, and then held at 130 ℃ for 30 minutes. Subsequently, the temperature was increased in steps of 10 ℃, with each temperature point being held for 30 minutes, until the final temperature of 300 ℃ was reached.

Molecular dynamics simulation

All the molecular dynamics (MD) simulations were performed by MD package GROMACS[57] Four models including 200 Na^+, 200 BF_4^- ions, 800 TEP molecules and 200 Na^+, 200 PF_6^- ions, 800 TEP molecules, and 200 Na^+, 200 BF_4^- ions, 800 TMP molecules and 200 Na^+, 200 PF_6^- ions, 800 TMP molecules were constructed. The forcefield parameters of TEP and TMP molecules were generated by LigParGen web server[58], except for their restrained electrostatic potential (RESP) atomic partial charges. These charges were assigned to each atom based on the electrostatic potential (ESP) charges obtained from the Multiwfn program[59]. The force field parameters for Na^+, BF_4^- and PF_6^- were obtained from Khan et al.[60]. These molecules were initially packed randomly within a cubic box of size 10×10×10 nm^3 using Packing Optimization for Molecular Dynamics Simulations (PACKMOL)[61].All the initial configurations were minimized through steepest descent with a convergence criterion of 500 kJ mol^{-1} nm^{-1}. All the systems were equilibrated using Berendsen barostat[62] to keep the pressure of 1 bar with a time constant of 3 ps. The production runs of 40 ns in NPT ensemble under Nóse-Hoover thermostat[63,64] and Parrinello-Rahman barostat[65] were conducted at 298 K, 313 K, 328 K, 343 K, 360 K and 380 K. For the radial distribution function (RDF) analysis, the last 5 ns simulations at 298 K were utilized. The last 5 ns simulations across all temperatures were dedicated to analyzing the desolvation energy of Na ions analysis. The van-der-Waals interactions was computed with a cutoff distance of 1.2 nm. The particle-mesh Ewald (PME)[66]method with a 1.2 nm real space cut-off was applied for the calculation of electrostatic interactions.

Density functional theory (DFT) simulations

The Gaussian 16 program[67] was employed to calculate the HOMO and LUMO level of $NaBF_4$, $NaPF_6$, TEP, TMP, DEC, and EC. In the DFT calculations, geometry optimization was carried out using Lee-Yang-Parr correlation functional (B3LYP)[68] at

6-311+G(d,p) level.

57 Lindahl, B. H. C. K. D. v. d. S. E. GROMACS 4: Algorithms for Highly Efficient, Load-Balanced, and Scalable Molecular Simulation. *J. Chem. Theory Comput.* **4**, 435-447 (2008).

58 Dodda, L. S., Cabeza de Vaca, I., Tirado-Rives, J. & Jorgensen, W. L. LigParGen web server: an automatic OPLS-AA parameter generator for organic ligands. *Nucleic Acids Res.* **45**, W331-W336 (2017).

59 Lu, T. & Chen, F. Multiwfn: a multifunctional wavefunction analyzer. *J. Comput. Chem.* **33**, 580-592 (2012).

60 Khan, M. S., Karatrantos, A. V., Ohba, T. & Cai, Q. The effect of different organic solvents and anion salts on sodium ion storage in cylindrical carbon nanopores. *Phys. Chem. Chem. Phys.* **21**, 22722-22731 (2019).

61 Martinez, L., Andrade, R., Birgin, E. G. & Martinez, J. M. PACKMOL: a package for building initial configurations for molecular dynamics simulations. *J. Comput. Chem.* **30**, 2157-2164 (2009).

62 Berendsen, H. J. C., Postma, J. P. M., van Gunsteren, W. F., DiNola, A. & Haak, J. R. Molecular dynamics with coupling to an external bath. *J. Chem. Phys.* **81**, 3684-3690 (1984).

63 Nosé, S., A molecular dynamics method for simulations in the canonical ensemble. *Molecular physics* 1984. 52(2): p. 255-268.

64 Hoover, W. G. Canonical dynamics: Equilibrium phase-space distributions. *Phys. Rev. A Gen. Phys.* **31**, 1695-1697 (1985).

65 Parrinello, M. & Rahman, A. Polymorphic transitions in single crystals: A new molecular dynamics method. *J. Appl. Phys.* **52**, 7182-7190 (1981).

66 Darden, T., York, D. & Pedersen, L. Particle mesh Ewald: An N·log(N) method for Ewald sums in large systems. *J. Chem. Phys.* **98**, 10089-10092 (1993).

67 Frisch, M. e.; Trucks, G.; Schlegel, H. B.; Scuseria, G.; Robb, M.; Cheeseman, J.; Scalmani, G.; Barone, V.; Petersson, G.; Nakatsuji, H. Gaussian 16. Gaussian, Inc. Wallingford, CT: 2016.

68 Lee, C., Yang, W. & Parr, R. G. Development of the Colle-Salvetti correlation-energy formula into a functional of the electron density. *Phys. Rev. B* **37**, 785-789 (1988).

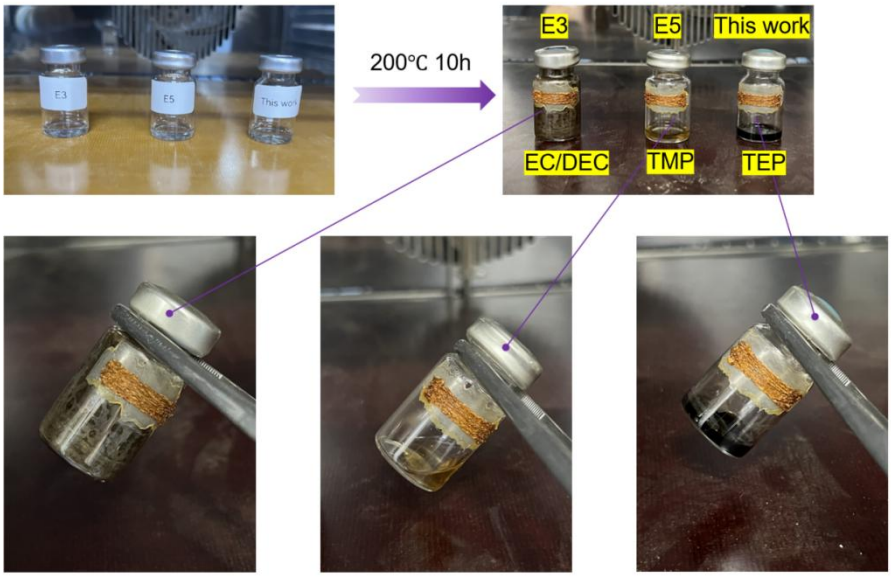

Figure S1. The heating experiment of E3, E5, and PNE electrolytes at 200℃.

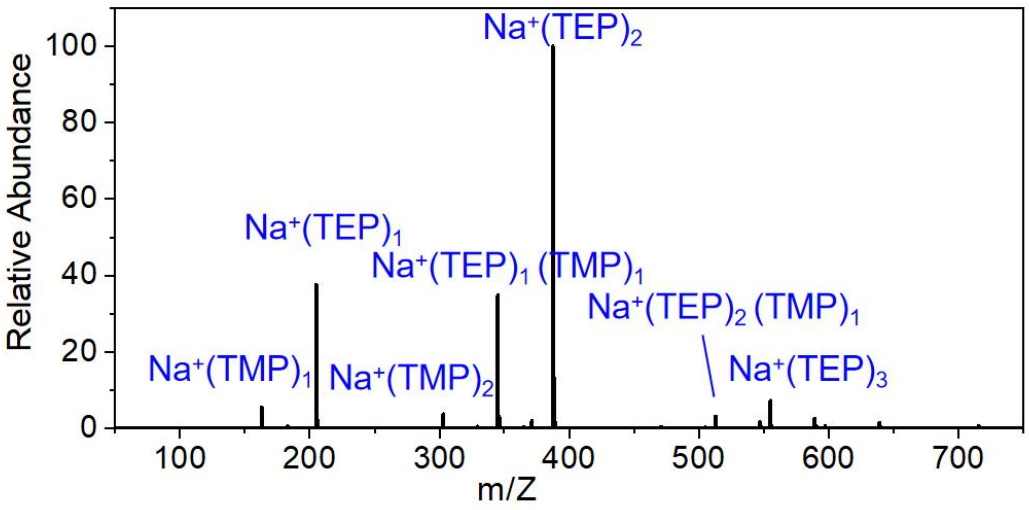

Figure S2. ESI-MS graphs for selected solution of 1.0 M $NaPF_6$ in TEP/TMP (1/1).

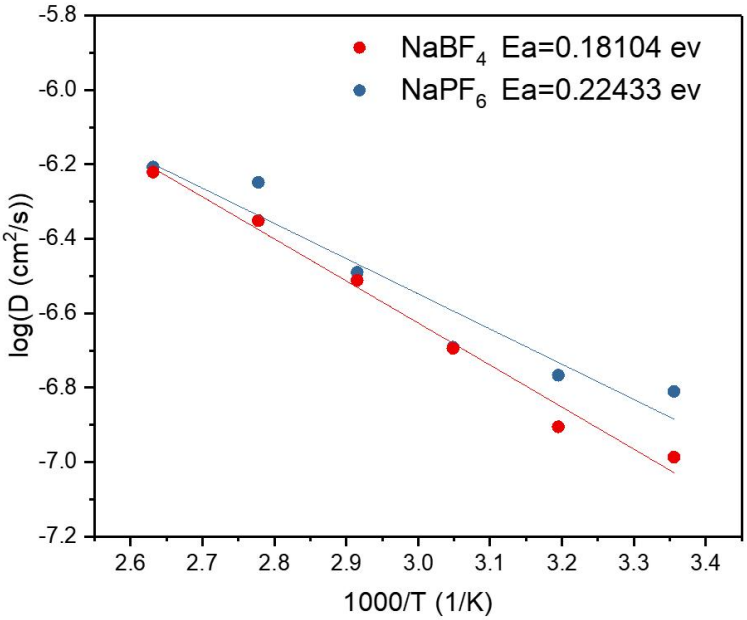

Figure S3. Activation energies of Na^+ desolvation (Ea) with $NaPF_6$ or $NaBF_4$ in TMP-based electrolyte.

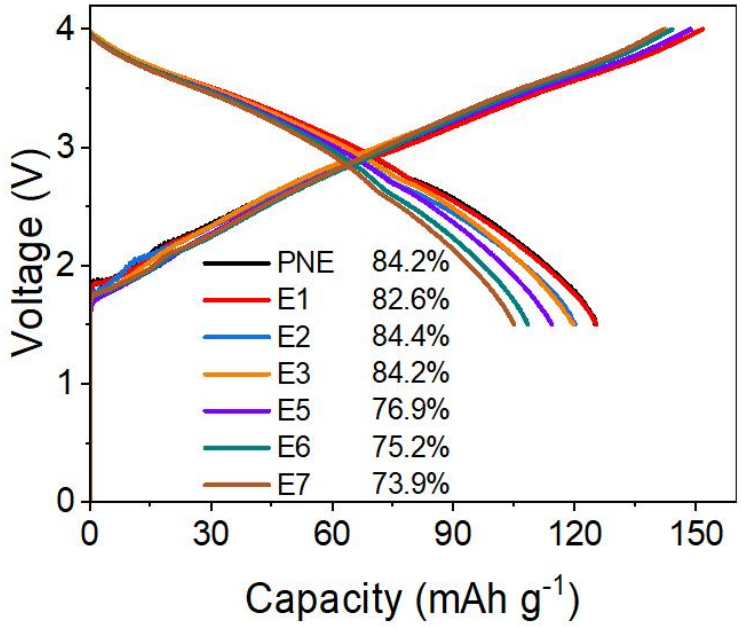

Figure S4. The first charge and discharge curves of a series of electrolytes in CNFM // HC 2032 coin cells.

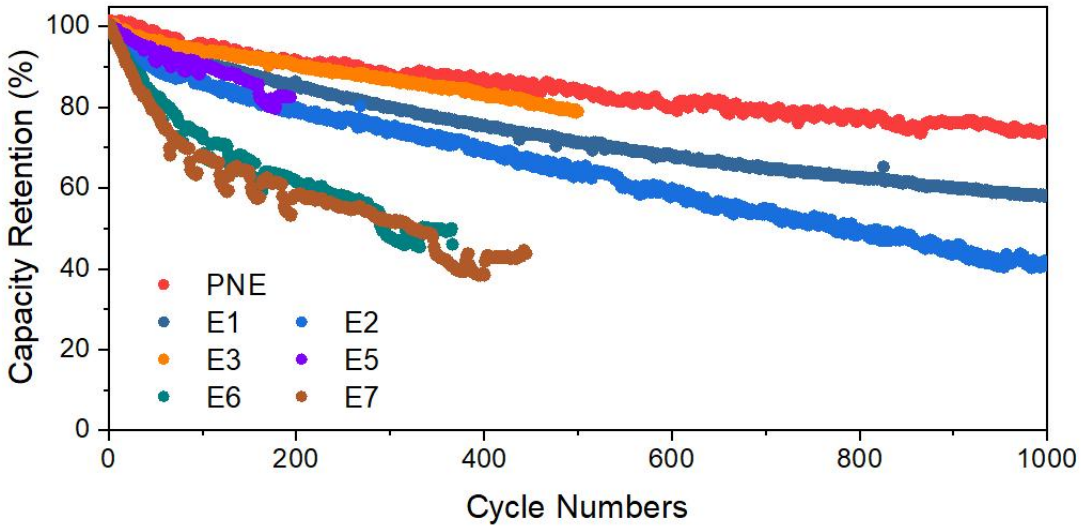

Figure S5. The electrochemical performance of O3-$NaCu_{1/9}Ni_{2/9}Fe_{1/3}Mn_{1/3}O_2$// HC coin cells with different electrolytes. Among them, E6 is 0.2M $NaPF_6$ and 0.8M $NaBF_4$ in TEP with 2% v/v VC, E7 is 0.8M $NaPF_6$ and 0.2M $NaBF_4$ in TEP with 2% v/v VC.

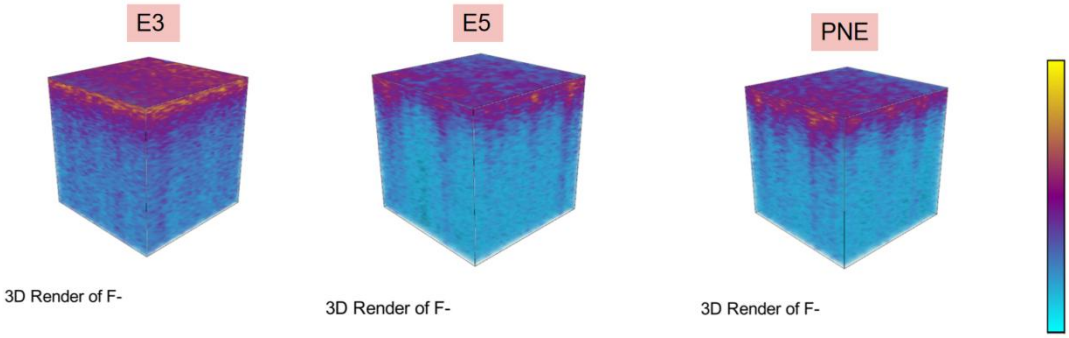

Figure S6. TOF-SIMS 3D figures of F^-. The colors on the color card from top to bottom indicate decreasing ion concentrations.

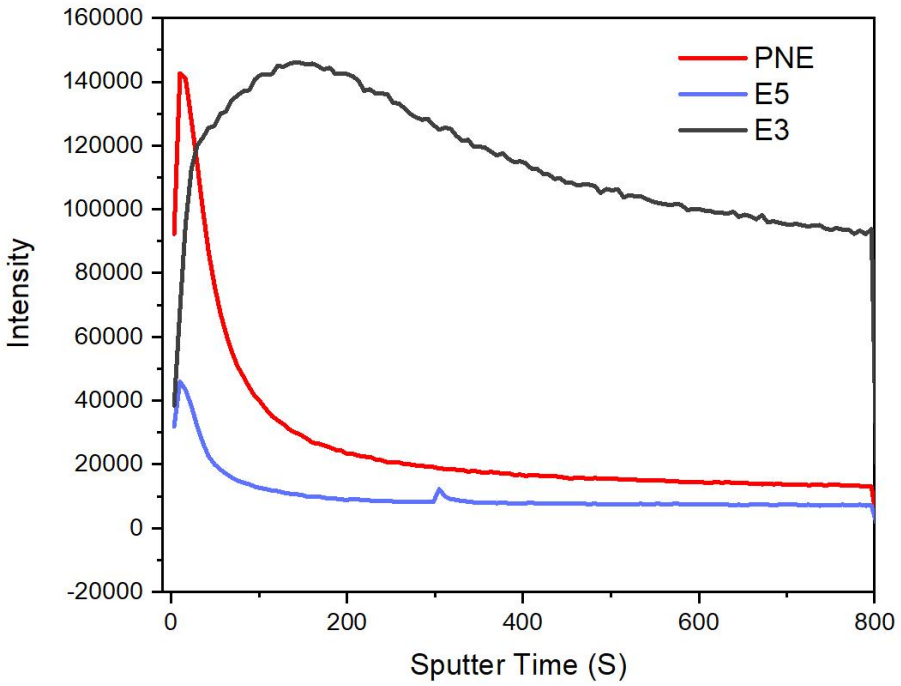

Figure S7. Normalized depth profiles of PO_2^- secondary ion fragments obtained from the anode of E3-, E5-, and PNE-based cell.

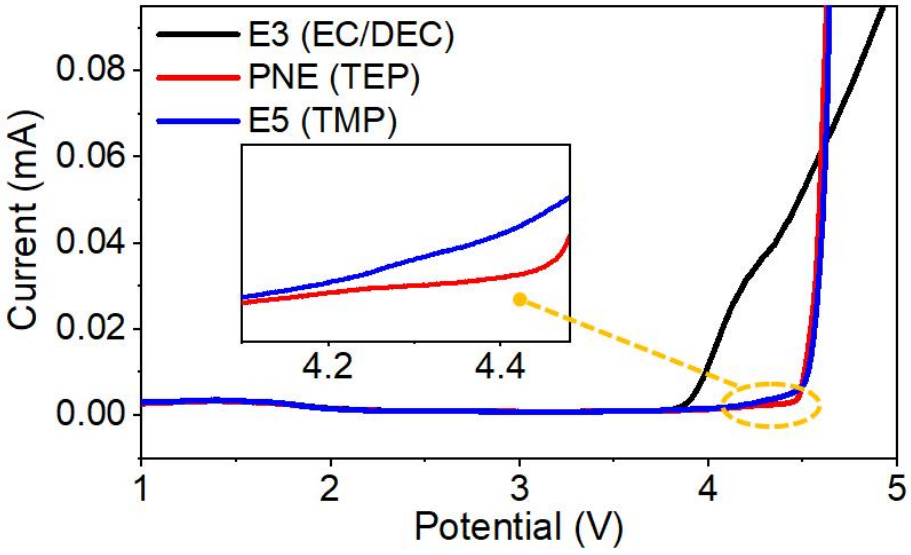

Figure S8. Linear sweep voltammetry (LSV) curves of E3, E5 and PNE.

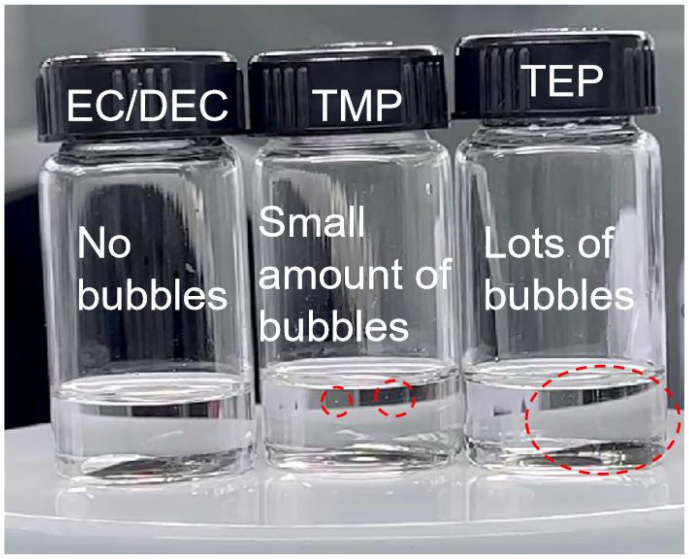

Figure S9. Immersion tests of sodium-deposited HC anode.

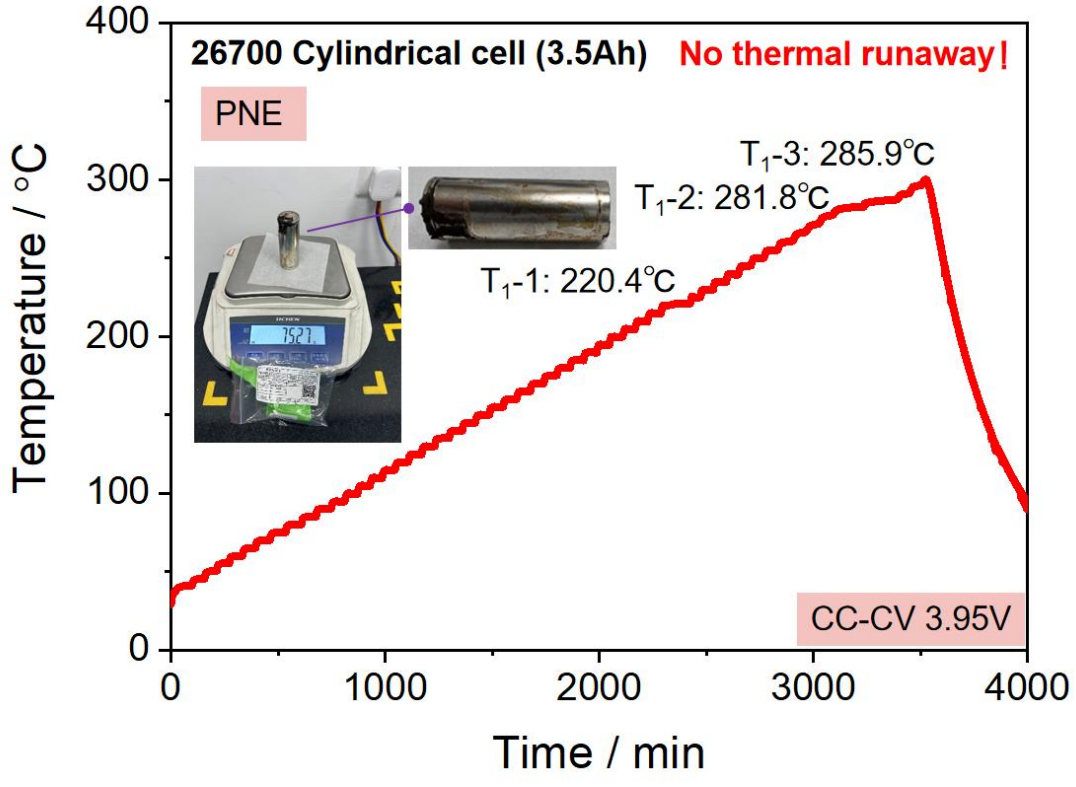

Figure S10. Accelerating Rate Calorimeter tests time-temperature curves of PNE-based 3.5Ah cylindrical cell.

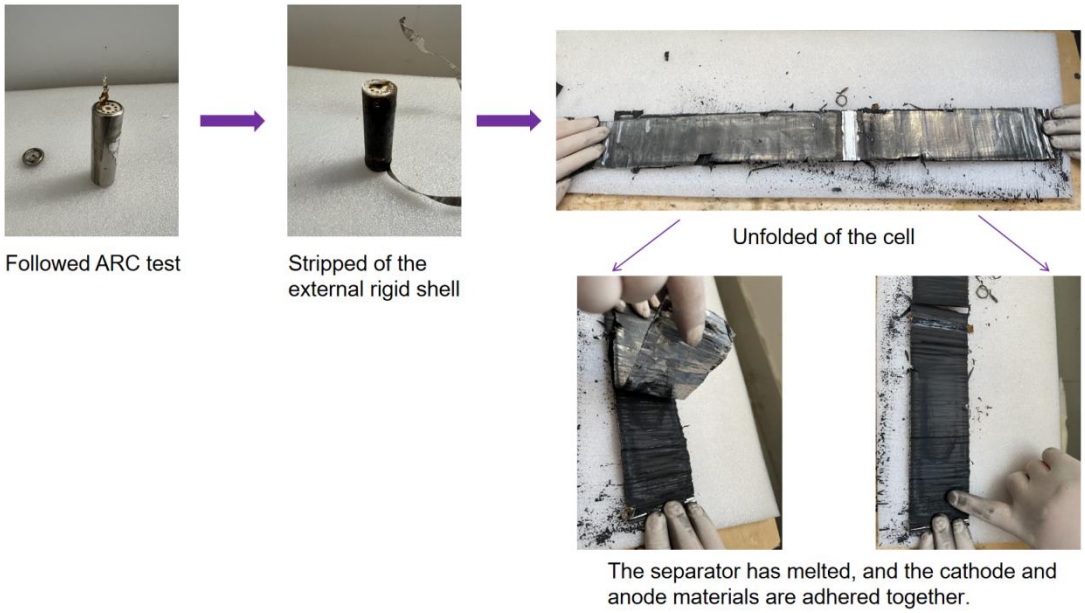

Figure S11. Disassembly of the PNE-based cell after the ARC test.

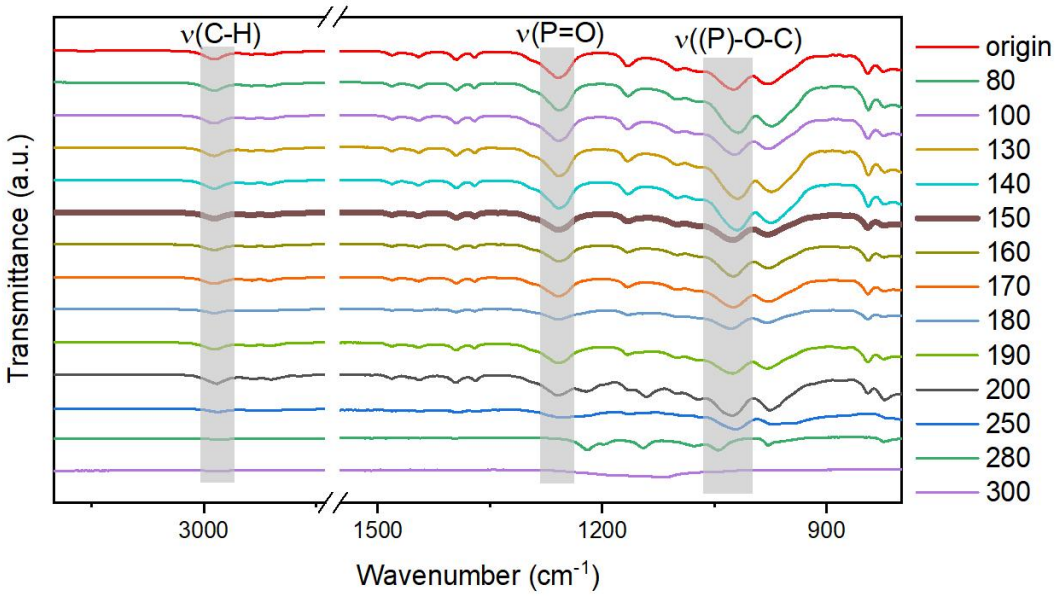

Figure S12. ATR-FTIR spectra of heated at different temperature Ploynonflytes (PNEs). The holding time for every temperature step is 30 minutes.

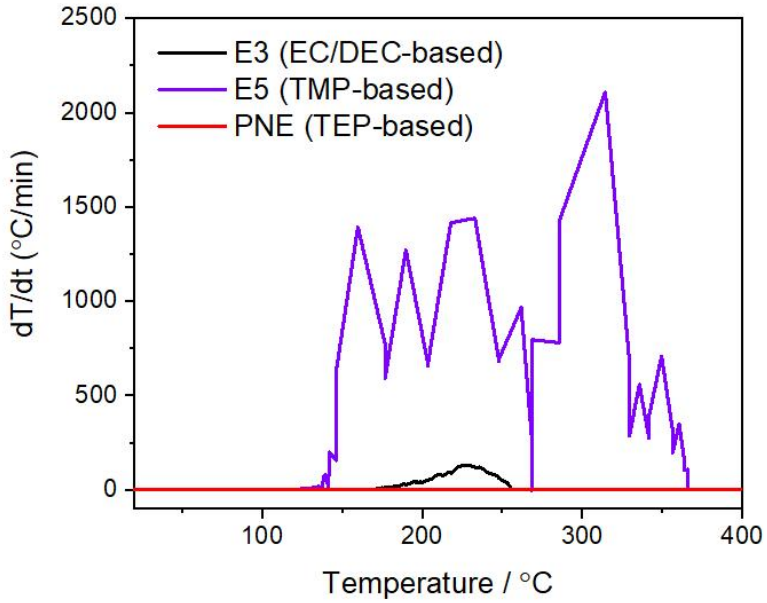

Figure S13. The heating rate curves of Accelerating Rate Calorimeter tests of E3-, E5- and PNE-based batteries.

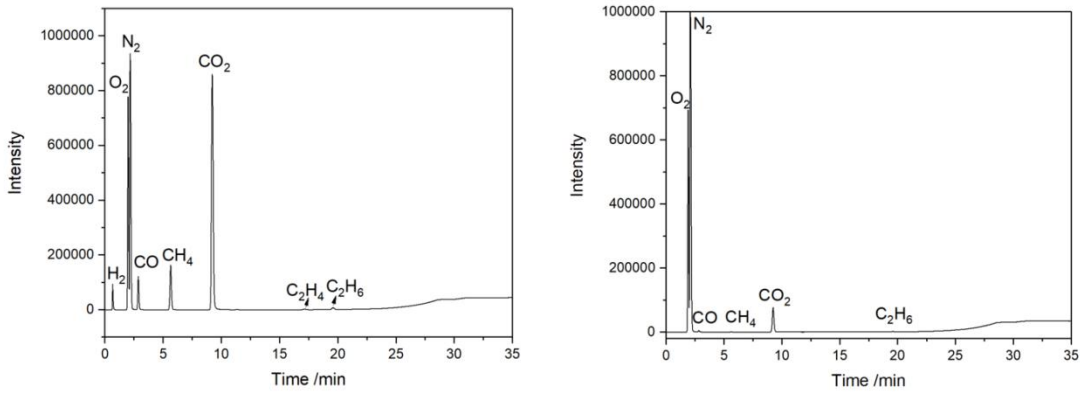

Figure S14. The original gas chromatographic collection data.

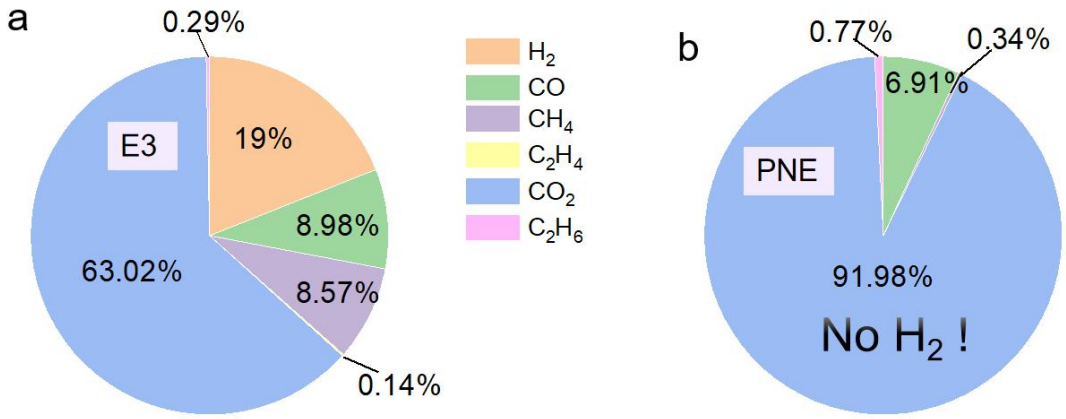

Figure S15. Analysis of gas producing from batteries after 60°C high-temperature storage by gas chromatography of E3 (a) and PNE (b).

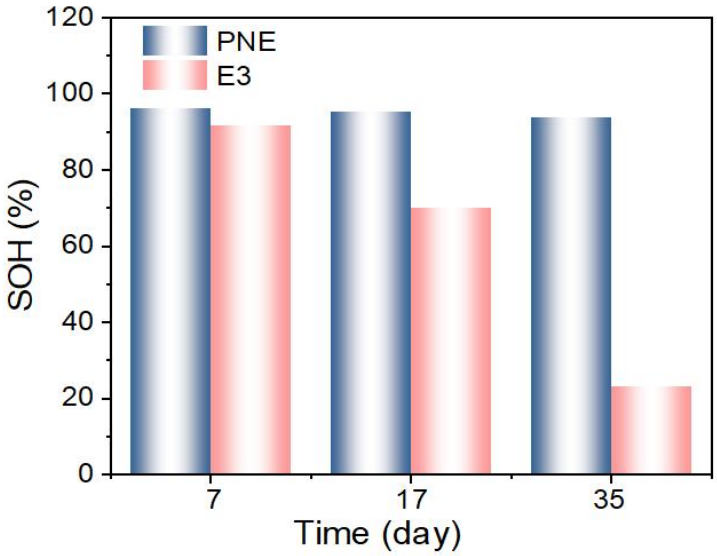

Figure S16. The high temperature storage performance at 60 ℃ of E3-based and PNE-based pouch cells.

Table S1. Battery-level safety studies detailed analysis and comparision with this work.

	Ref.	Capacity (Ah)	Safe test	Method
Lithium	Ref.2	0.9	ARC test discussion	HCE
	Ref.7	3.5	Passed nail penetration test	Fluorinated electrolyte
	Ref.8	2	Passed nail penetration test	HCE
	Ref.9	lithium metal coin cell	ARC test discussion	Polymer electrolyte
	Ref.10	0.5	ARC test discussion + passed nail penetration test	Gel polymer electrolyte
	Ref.19	1.2	Passed the nail penetration test	LHCE + fluorinated
	Ref.32	1.1	ARC test discussion + passed nail penetration test	Fluorinated electrolyte
	Ref.41	2.2	Passed nail penetration test	Ionic liquid electrolyte
	Ref.42	0.22	ARC test discussion	Fluorinated electrolyte
Sodium	Ref.43	1	ARC test discussion	Solid-state reaction synthesis of $Na_xNi_{1/3}Fe_{1/3}Mn_{1/3}O_2$ cathode materials improves battery safety
	This work	**1.45 Ah & 3.5Ah cylindrical battery**	**Nail penetration test no fire, no smoke, no explosion, passed the 300 °C Accelerating Rate Calorimeter (ARC) and thermal abuse tests.**	**Polymerizable and non-flammable electrolyte (PolyNonflyte or PNE)**

Table S2. The electrolyte components of the designed electrolyte and comparative samples. The proportions of solvents or additives involved are all volume ratios.

Electrolyte number abbreviation	Electrolyte composition
E1	1.2M $NaBF_4$ in TEP+2% VC
E2	1.2M $NaPF_6$ in TEP+2% VC
E3	1.2M $NaPF_6$ in EC/DEC (1/1) +2% VC
PNE	0.2M $NaPF_6$+1.0M $NaBF_4$ in TEP+2% VC
E5	0.2M $NaPF_6$+1.0M $NaBF_4$ in TMP+2% VC
E6	0.2M $NaPF_6$+0.8M $NaBF_4$ in TEP+2% VC
E7	0.8M $NaPF_6$+0.2M $NaBF_4$ in TEP+2% VC

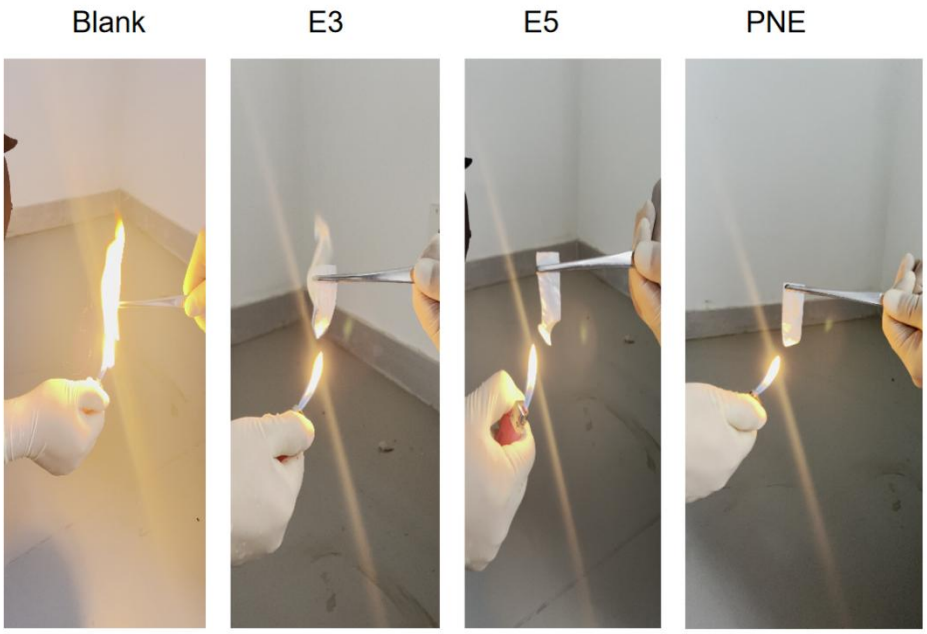

Video S1-S4. Ignition experiment videos of fresh separator (Video S1) and the separators immersed in E3 (Video S2), E5 (Video S3) and PNE (Video S4).

Video S5. Nail penetration test of E3 (EC/DEC-based) with 18650 cylindrical cell.

Video S6. Nail penetration test of E5 (TMP-based) with 18650 cylindrical cell.

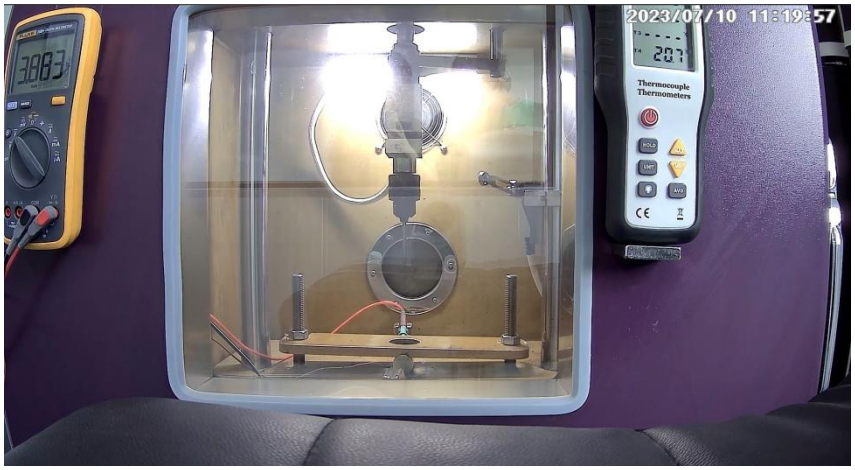

Video S7. Nail penetration test of PNE (TEP-based) with 26700 cylindrical cell.

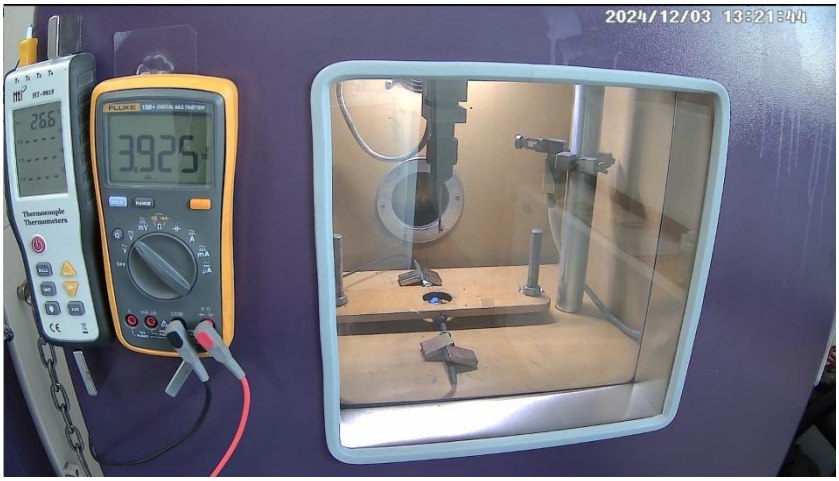

Video S8. Nail penetration test of PNE (TEP-based) with 18650 cylindrical cell.

Video S9. Immersion tests of sodium-deposited HC anode. (Left) EC/DEC; (Middle) TMP; (Right) TEP.